Stem Cell Reports
Article

ISSCR

OPEN ACCESS

Force and Calcium Transients Analysis in Human Engineered Heart Tissues Reveals Positive Force-Frequency Relation at Physiological Frequency

Umber Saleem,[1,3] Ingra Mannhardt,[1,3] Ingke Braren,[2,3] Chris Denning,[4] Thomas Eschenhagen,[1,3] and Arne Hansen[1,3,*]

[1]Department of Experimental Pharmacology and Toxicology, University Medical Center Hamburg-Eppendorf, 20246 Hamburg, Germany
[2]Vector Facility, University Medical Center Hamburg-Eppendorf, 20246 Hamburg, Germany
[3]German Center for Cardiovascular Research (DZHK), Partner Site Hamburg/Kiel/Lübeck, 20246 Hamburg, Germany
[4]Wolfson Centre for Stem Cells, Tissue Engineering and Modelling, Centre for Biomolecular Sciences, University of Nottingham, University Park, Nottingham NG7 2RD, UK
*Correspondence: ar.hansen@uke.de
https://doi.org/10.1016/j.stemcr.2019.12.011

SUMMARY

Force measurements in *ex vivo* and engineered heart tissues are well established. Analysis of calcium transients (CaT) is complementary to force, and the combined analysis is meaningful to the study of cardiomyocyte biology and disease. This article describes a model of human induced pluripotent stem cell cardiomyocyte-derived engineered heart tissues (hiPSC-CM EHTs) transduced with the calcium sensor GCaMP6f followed by sequential analysis of force and CaT. Average peak analysis demonstrated the temporal sequence of the CaT preceding the contraction twitch. The pharmacological relevance of the test system was demonstrated with inotropic indicator compounds. Force-frequency relationship was analyzed in the presence of ivabradine (300 nM), which reduced spontaneous frequency and unmasked a positive correlation of force and CaT at physiological human heart beating frequency with stimulation frequency between 0.75 and 2.5 Hz (force +96%; CaT +102%). This work demonstrates the usefulness of combined force/CaT analysis and demonstrates a positive force-frequency relationship in hiPSC-CM EHTs.

INTRODUCTION

Analysis of the contractile force of heart muscle trabeculae from laboratory animals or human hearts has been established for decades and has substantially contributed to the understanding of mechanisms and genes involved in force regulation. During the last decade, different technologies were established to generate contractile force in human induced pluripotent stem cell cardiomyocyte-derived engineered heart tissue (hiPSC-CM EHT) (Bielawski et al., 2016; Cashman et al., 2016; Hinson et al., 2016; Jackman et al., 2016; Kensah et al., 2013; Leonard et al., 2018; Mannhardt et al., 2016; Mills et al., 2017; Nunes et al., 2013; Ronaldson-Bouchard et al., 2018; Ruan et al., 2016; Tiburcy et al., 2017; Tulloch et al., 2011; Zhao et al., 2019). Analysis of contractile force has been instrumental in the development of EHT models because it allows the force response to be compared with human heart tissue. The challenge of interpreting force data is related to their complex nature, i.e., alteration of numerous targets related to myofilaments, calcium-handling proteins, and other targets that affect force development. The combination of force analysis with readouts of cytoplasmic increase in calcium concentration (calcium transient, CaT) during systole and decrease during diastole is therefore a meaningful extension of contractility assays. Such assays for heart muscle trabeculae are established with aequorin (Gwathmey and Hajjar, 1990; Perreault et al., 1992) or calcium-sensitive dyes (Brixius et al., 2003, 2002; Haizlip et al., 2015). In analogy, we and others (Nunes et al., 2013; Rao et al., 2018; Ronaldson-Bouchard et al., 2018; Ruan et al., 2016; Stoehr et al., 2014; Zhao et al., 2019) have established CaT measurements in different EHT models with calcium-sensitive dyes or genetically encoded calcium sensors (GECIs) for the characterization of EHTs.

The adaptation of force to changes in beating frequency (force-frequency relationship [FFR] or Bowditch effect) is well described for human myocardium (Mulieri et al., 1992; Pieske et al., 1999; Schmidt et al., 1995). Mechanistically, the integrated dynamic balance of the intracellular calcium concentration is key to this phenomenon (Bers et al., 2014; Klabunde, 2012; Krishna et al., 2013). With increasing stimulation frequency, calcium influx via the L-type calcium channels (LTCCs) and calcium uptake into the sarcoplasmic reticulum exceed calcium efflux via the sodium-calcium exchanger. In consequence, the amplitude of the CaT increases in a frequency-dependent manner. Important characteristics of this mechanism across several mammalian species are a positive correlation between both force and CaT amplitude with frequency at beating rates close to the physiological heart rate of the respective species. At higher frequencies, a dissociation between further increasing CaT amplitudes and a secondary-phase negative FFR was described (Endoh, 2004; Mulieri et al., 1992; Pieske et al., 1999). In hiPSC-EHT models, the absence of a positive FFR was interpreted as an indicator of immaturity, and a positive correlation could be demonstrated only in the presence of electrical conditioning

(Ronaldson-Bouchard et al., 2018; Zhao et al., 2019) or defined serum-free medium conditions (Tiburcy et al., 2017).

In this article, we demonstrate an extension of video-optical analysis of contractile force in hiPSC-CM EHTs by sequential measurement of GCaMP6f-mediated fluorescence intensity, a surrogate for CaT, as a robust model to study cardiac physiology and pharmacology. Specifically, we demonstrate canonical effects of indicator compounds on CaT and force. Furthermore, we assess the correlation of CaT and force amplitude at physiological human heart rates by reducing spontaneous baseline frequency with the I_f current inhibitor ivabradine. Under this condition, we unmasked a positive force- and CaT-frequency relationship between 0.75 and 2.5 Hz in the absence of electrical conditioning or defined serum-free medium. In aggregate, the data present an innovative model to analyze CaT and force in EHTs to study physiological mechanisms and pharmacological effects.

RESULTS

Specificity of Fluorescence Signal

Human iPSC-CMs were efficiently transduced with lentivirus encoding either GCaMP5G or GCaMP6f in a two-dimensional (2D) monolayer, demonstrated by a bright GFP fluorescence signal during contraction (Figures 1A and 1B, and Videos S1, S2, S3, and S4). CaT and force were recorded from hiPSC-CM EHTs transduced with GCaMP5G or GCaMP6f. In GCaMP5G EHTs, kinetics of time-to-peak CaT ($TTP_{-80\%,CaT}$; 0.181 ± 0.004 s) was 28% longer than time-to-peak force ($TTP_{-80\%,force}$; 0.141 ± 0.001 s), and decay time of the CaT ($DT_{80\%}$; 0.329 ± 0.003 s) was 99% longer than relaxation time for force ($RT_{80\%,force}$; 0.165 ± 0.002 s; Figure 1C, left, Figure S1A). This resulted in a clockwise orientation of the force-calcium loop (Figure 1C, right), and a faster contraction phase indicated by lower density of the data points marks the beginning of the loop. In GCaMP6f EHTs, $TTP_{-80\%,CaT}$ was 20% shorter than $TTP_{-80\%,force}$ (0.116 ± 0.004 s versus 0.145 ± 0.005 s), and $DT_{80\%,CaT}$ was 16% longer than $RT_{80\%,force}$ (0.173 ± 0.007 s versus 0.149 ± 0.003 s). This characteristic resulted in superimposition of the terminal phases of CaT and contraction (Figure 1D, left, Figure S1B) and a counterclockwise orientation of the force-calcium loop (Figure 1D, right). We therefore focused on GCaMP6f for further characterization. Average force peaks of GCaMP5G- and GCaMP6f-transduced EHTs showed an overlap, while CaT average peaks demonstrated slower on-and-off kinetics for GCaMP5G (Figure S1C). Original CaT recordings showed strong signals and weak background noise. Signal-to-noise ratio was calculated as 64.2 ± 8.6, SEM (N: number of EHTs = 12 EHT recordings).

Histologically, GCaMP6f (transduced at the time of casting) did not interfere with myofilament organization or cellular alignment along the long axis of the EHT, as indicated by cardiac alpha-actin staining (Figure S2B). Staining for GFP revealed transduction of 20%–40% of hiPSC-CMs within the EHT (Figures S2C and S2D).

To demonstrate the dependency of CaT amplitude on GCaMP6f expression, EHTs were transduced with GCaMP6f-AAV6-particles at two different multiplicities of infection (MOI, 7×10^4 and 7×10^5). Analysis of CaT and force (Figure 1E) revealed higher CaT amplitude for 7×10^5 MOI transduction (10,885 versus 5,192 AU, Figure S1D), while force was not different (0.088 versus 0.086 mN, Figure S1). GCaMP6f EHTs were also analyzed at extracellular calcium concentrations of 0.6 and 1.8 mM. At 1.8 mM calcium, CaT amplitude was 185% higher (15,128 versus 5,318 AU) and force amplitude was 154% higher (0.165 versus 0.065 mN, Figures 1F and S1E) compared with 0.6 mM calcium.

Motion artifacts are a possible limitation of CaT recordings in auxotonic or isotonic contracting muscle tissues/cells (Kaestner et al., 2014). To minimize the contribution of motion artifacts, GCaMP6f fluorescence was recorded at a rectangular window of 0.1 × 0.4 mm in the center of the EHT where motion during contraction is the least (Figure S2E). To understand the contribution of motion artifacts on CaT signals, autofluorescence was recorded in non-transduced EHTs (Figure 2A) and GFP-transduced EHTs (Figure 2B). Peak amplitude of the autofluorescence or GFP fluorescence signals was more than 10-fold smaller than GCaMP5G or GCaMP6f signal intensities (which were in the range of 5,000–25,000 AU), and it was superimposed with the contraction twitch (Figures 2A and 2B, left). This resulted in a symmetrical loop with similar data point density for the contraction and relaxation phases of force-fluorescence loops (Figure 2A, right) or linear force-light dependency (Figure 2B, right). This supports the finding that the temporal sequence of CaT and force and the force-calcium loop shape (Figures 1C and 1D) represent specific signals. To determine whether the absence of contractile motion would affect CaT amplitude, GCaMP6f-EHTs were generated on hollow polydimethylsiloxane (PDMS) posts according to a previously established protocol that would enable stiffening of the flexible posts and therefore abrogate EHT movement (Hirt et al., 2012). Recording of CaT and force for time-matched controls (TMCs) revealed no change during the time course of the experiment (Figure 2C, left). For the experimental group, introduction of metal braces reduced shortening/post deflection to nominally zero with minor reduction of CaT, which was reversed after removal of the metal braces (Figure 2C, right). In a second experiment to analyze CaT in the absence of contraction, GCaMP6f-EHTs were analyzed in the presence of 2,3-butanedione

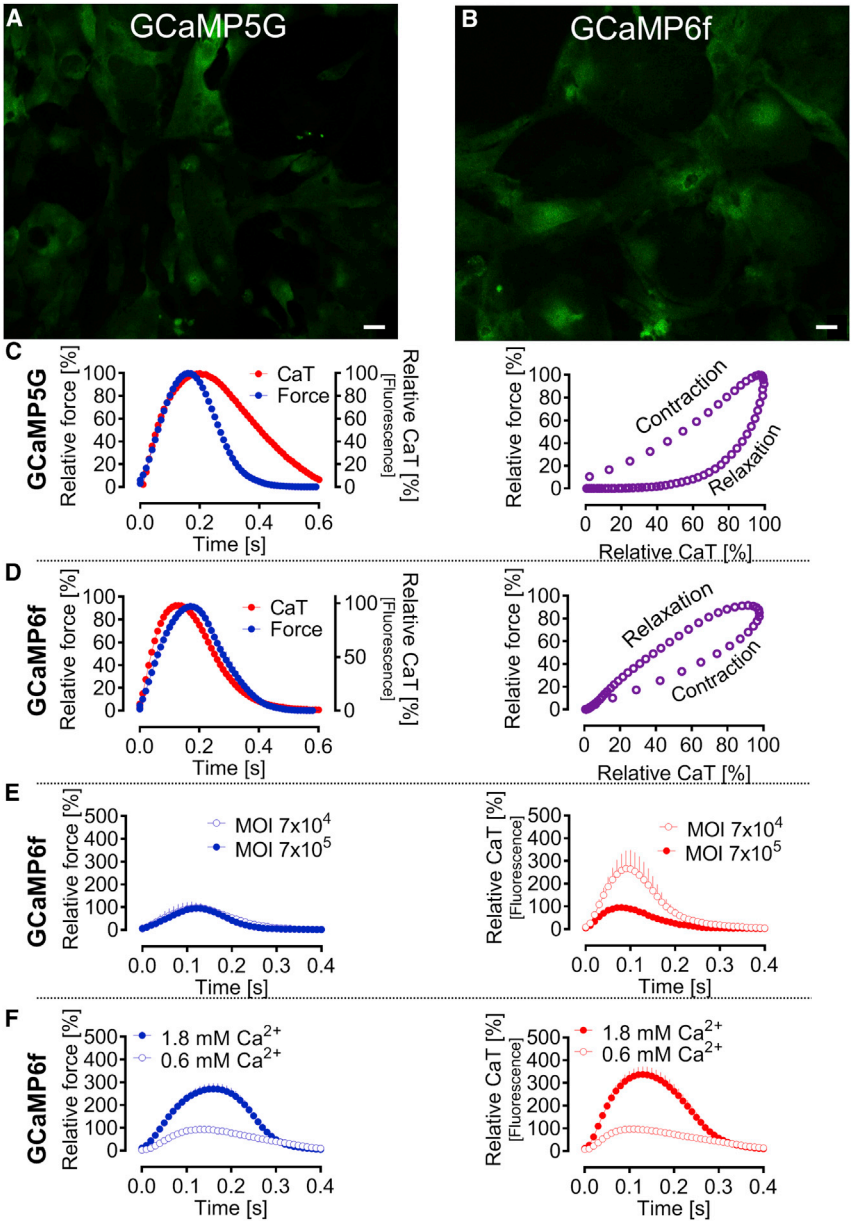

Figure 1. Optimization of CaT Measurements by Using GCaMPs

(A and B) Representative images of hiPSC-CMs after lentiviral transduction with (A) GCaMP5G and (B) GCaMP6f. Videos were recorded from beating cardiomyocytes with a confocal microscope. The images display cardiomyocytes during contraction when GCaMP fluorescence intensity is high (scale bar, 20 μm).

(C) Average normalized CaT and force peaks of hiPSC-CM EHTs after lentiviral transduction with GCaMP5G (left). Depiction of the same data as a force-calcium loop, n = 5; 1; 1 (right).

(D) Average normalized CaT and force peaks of hiPSC-CM EHTs after lentiviral transduction with GCaMP6f (left). Depiction of the same data as a force-calcium loop, n = 25; 3; 4 (right).

(E) Average normalized force (left) and CaT (right) peaks of hiPSC-CM EHTs virally transduced with GCamP6f (AAV6, MOI 7 × 10^4 and 7 × 10^5, n = 3; 1; 1).

(F) Average normalized force (left) and CaT (right) peaks of hiPSC-CM EHTs virally transduced with AAV6- and LV-GCaMP6f at 0.6 and 1.8 mM Ca^{2+} (n = 21; 3; 3). Replicates are indicated as number of independent samples; number of hiPSC cell lines; number of repeated measurements (N; nl; nm); N was used for statistics.

Data are depicted as means ± SEM except for the force-calcium loops. Measurements were done in modified Tyrode's solution at 1.8 mM Ca^{2+} under electrical stimulation of 1.5 Hz (C and D), 2.0 Hz (E), and 1.5 Hz for N = 17 and 2.0 Hz for N = 4 (F). See also Figure S1.

monoxime (BDM; 10 mM; experiments with blebbistatin were not successful because of strong autofluorescence; Képiró et al., 2014). TMCs for this experiment showed again no significant changes in CaT, but force decreased by 21% (Figure 2D, left). BDM reduced force by −85% and CaT by −44%. The reason for the BDM-induced reduction of CaT is not clear, but the low potency of BDM and thus the high working concentration likely result in multiple off-target effects (Biermann et al., 1998). Reproducibility of force and CaT recordings was analyzed by three repetitive measurements with 3 h intervals. While force values did not differ (0.238 ± 0.008, 0.230 ± 0.007, 0.230 ± 0.007, mN ± SEM, N = 16), CaT amplitudes showed 10% decline (8,003 ± 344, 7,241 ± 327, 7,293 ± 320, AU ± SEM, N = 15), likely a consequence of photo bleaching as recently reported for GCaMP6f (Li et al., 2019) (Figures S2F and S2G). This finding implicates that the effect sizes for the repetitive CaT recording experiments might be slightly underestimated.

Compound-Specific Effects

A set of indicator compounds was chosen to validate this test system. The results are demonstrated in Figures 3, S3, and S4 and Table S1. The β-adrenergic agonist isoprenaline

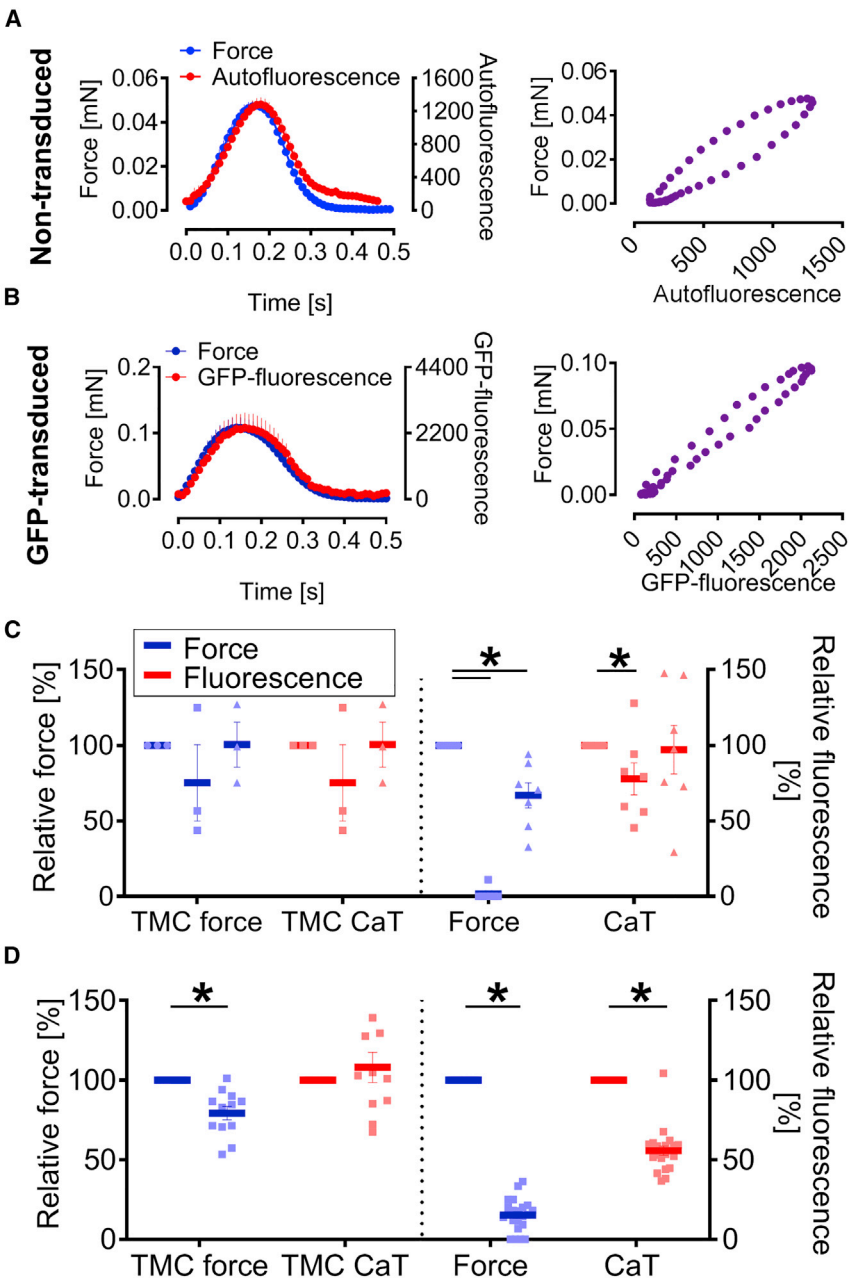

Figure 2. Motion Artifact Analysis of CaT Measurements

(A) (Left) Average contraction force and fluorescence intensity peaks of non-transduced hiPSC-CM EHTs. (Right) Force-calcium loops of data depicted on the left, n = 5; 1; 2; pacing frequency 2.0 Hz.

(B) (Left) Average contraction force and fluorescence intensity peaks of hiPSC-CM EHTs transduced with GFP. (Right) Force-calcium loops of data depicted on the left, n = 13; 2; 3; pacing frequency 1.5 Hz.

(C) Scatterplot depictions of contraction force (blue) and fluorescence intensity (red) of EHTs transduced with GCaMP6f at baseline (●) and in the presence (■) and absence (▲) of metal braces, n = 7; 1; 1 (right); pacing frequency 1.5 Hz; data are normalized to own baseline. Statistical analysis was performed on data normalized to the average baseline; two-way ANOVA with Tukey's multiple comparisons posttest, *p < 0.05. Left shows time-matched controls (TMCs).

(D) Scatterplot depictions of contraction force (blue) and fluorescence intensity (red) of GCaMP6f-transduced EHTs in the presence and absence of BDM (10 mM) in modified Tyrode's solution, at 0.4–0.6 mM Ca^{2+} for hiPSC cell line 2, and 0.8 mM Ca^{2+} for hiPSC cell line 3, n = 22; 2; 4; pacing frequency 2.0 Hz; data are normalized to own baseline. Statistical analysis was performed on data normalized to the average baseline, two-way ANOVA with Bonferroni's multiple comparisons posttest, *p < 0.05. Left shows TMCs. Replicates are indicated as number of independent samples; number of hiPSC cell lines; number of repeated measurements (N; nl; nm); N was used for statistics.

Measurements for (A), (B), and (C) were done in modified Tyrode's solution at 1.8 mM Ca^{2+}. Data are depicted as means ± SEM or means only for loops. See also Figure S2.

(10 nM) led to an increase in force (+51%) and reduction in $TTP_{-80\%,force}$ and $RT_{80\%,force}$ (−17%) as expected. This was accompanied by an increase in CaT amplitude (+64%) and reduction in $TTP_{-80\%,CaT}$ and $RT_{80\%,CaT}$ (−17%; 14%). Force-calcium loops demonstrated higher force and CaT maximum. The LTCC inhibitor nifedipine (10, 30, and 100 nM) led to a concentration-dependent decrease in force (−67%) and CaT (−77%). Also $TTP_{-80\%,force}/TTP_{-80\%,CaT}$ and $RT_{80\%,force}/DT_{80\%,CaT}$ were significantly reduced (−29%/−17% and −22%/−21%, respectively; 100 nM). Some EHTs stopped beating at 100 nM (Figure S3B). Force-calcium loops demonstrated smaller force and CaT amplitude values. The LTCC agonist Bay K-8644 (300 nM) led to an increase in force (+71%) and $RT_{80\%,force}$ (+86%). This was accompanied by an increase in $DT_{80\%,CaT}$ (+74%). CaT amplitude increased at 30 and 100 nM (+53%, +62%) but not at 300 nM. Force-calcium loops demonstrated higher amplitudes for force and CaT at 30 nM and more force for a given calcium at 300 nM. The sodium/potassium ATPase inhibitor digoxin increased force and CaT at 300 nM

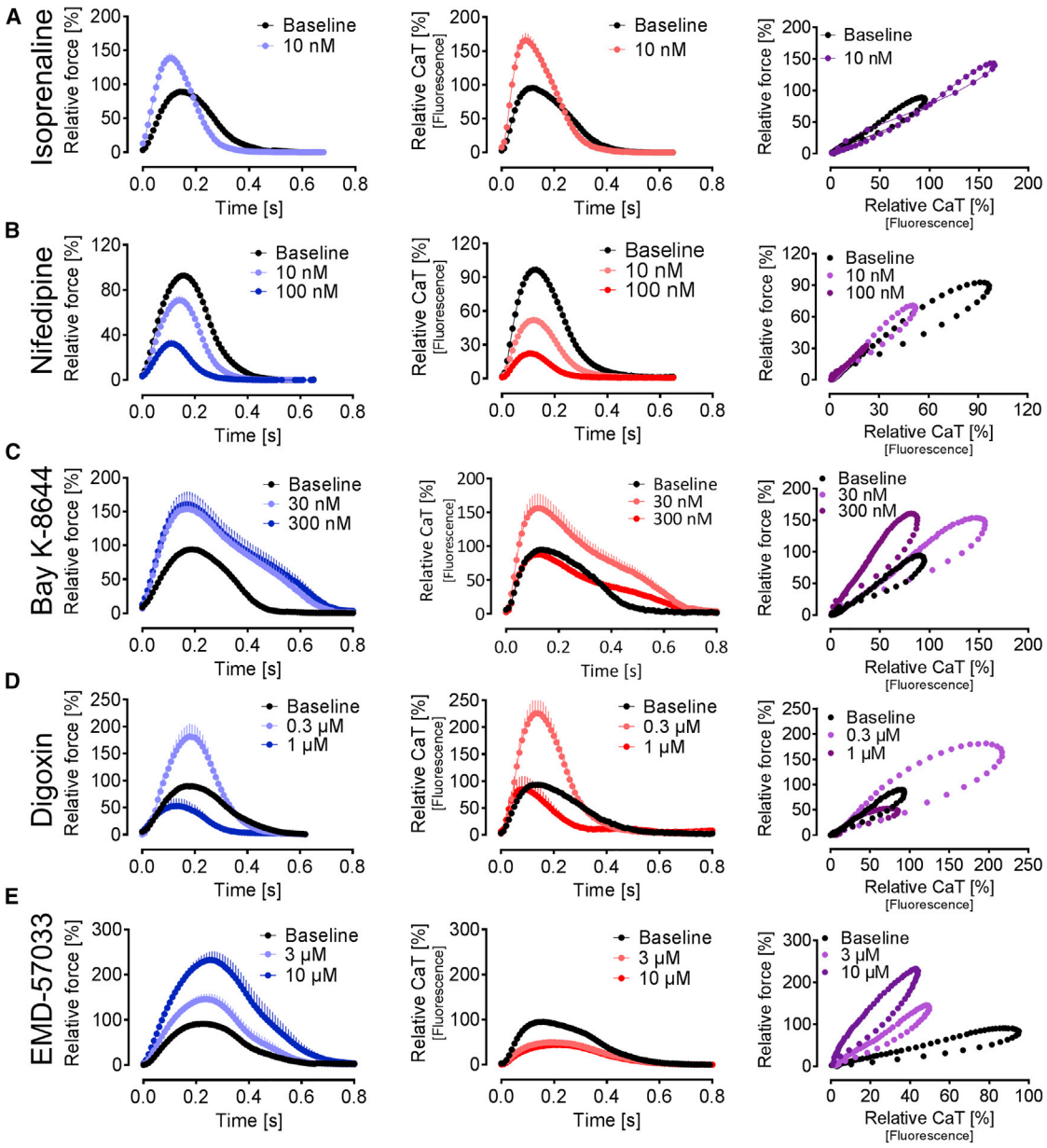

Figure 3. Force and CaT Analysis of hiPSC-CM EHTs Using Indicator Compounds

Average peaks of contraction force (blue, left) and CaT (red, middle) and force-calcium loops (purple, right) of hiPSC EHTs at baseline (black) and with compound incubation (blue/red/purple). Depicted are the relative effects in percentage of baseline (mean ± SEM or mean only for loops) in modified Tyrode's solution. Positive inotropic compounds (A and C–E) were analyzed at submaximal Ca^{2+} (hiPSC cell line 1, 1.0 mM except Bay K-8644 at 0.6 mM; hiPSC cell line 2, 0.5 mM; hiPSC cell line 3, 0.6 mM) and the negative inotropic compound (B) was measured at 1.8 mM Ca^{2+} in all cell lines. All measurements were performed under electrical stimulation. (A) Isoprenaline: n = 25; 3; 4; 1.5 Hz (N = 2) and 2.0 Hz (N = 23). (B) Nifedipine: n = 26; 3; 4; 1.5 Hz (N = 26). (C) Bay K-8644: n = 23; 3; 4; 1.0 Hz (N = 16) and 1.5 Hz (N = 7); for N = 4, pacing frequency was reduced from 1.5 to 1.0 Hz during drug exposure because of loss of capture of EHTs at 1.5 Hz. (D) Digoxin: n = 24; 3; 4; 1.0 Hz (N = 24). (E) EMD-57033: n = 22; 3; 3; 1.5 Hz (N = 17) and 1.0 Hz (N = 5). Replicates are indicated as number of independent samples; number of hiPSC cell lines; number of repeated measurements (N; nl; nm); N was used for statistics. See also Figures S3 and S4.

(+87%, +142%), accompanied by a reduction in $RT_{80\%,force}$ and $DT_{80\%,CaT}$ (−19%, −27%). At 1 μM, digoxin led to a reduction in force by −50% and no change in CaT (−7%), compatible with its known toxicity at higher concentrations. Force-calcium loops demonstrated a harmonic increase in force and CaT at 300 nM and a drastic reduction in force at 1 μM. The myofilament calcium sensitizer EMD-57033 led to an increase in force (+130%) and $TTP_{-80\%,force}$ (+15%) at 10 μM. CaT amplitude decreased (−50%) and $TTP_{-80\%,CaT}$ increased (+21%). Force-calcium loops demonstrated a strong increase in force per calcium for contraction and relaxation and a higher force amplitude.

Force-Frequency Relationship

In recent studies, we were not able to demonstrate a positive FFR in hiPSC-CM EHTs (Mannhardt et al., 2016), whereas others demonstrated FFR in the presence of electrical conditioning (Ronaldson-Bouchard et al., 2018; Zhao et al., 2019) or defined serum-free medium conditions (Tiburcy et al., 2017). We hypothesized that a positive FFR in EHTs may be masked by a high spontaneous beating rate. Spontaneous beating of hiPSC-CMs is dependent on the I_f current (Mannhardt et al., 2016); hence, we evaluated FFR in hiPSC-CM EHTs in the presence of ivabradine (300 nM), which reduces spontaneous beating frequencies to 25% (Mannhardt et al., 2016). In the presence of ivabradine, hiPSC-CM EHTs could be paced at the physiological human heart rate, between 0.75 and 2.5 Hz (Figure 4). Between 0.75 and 2.0 Hz, the increase in stimulation frequency was accompanied by an increase in force (+96%) and CaT (97%). At higher frequencies, up to 2.5 Hz, force values decreased (2.5 Hz: +82%). In contrast, CaT further increased (2.5 Hz: 102%) (Figures 4A and 4B). In parallel, $TTP_{-80\%,force}$, $TTP_{80\%,CaT}$, $RT_{80\%,force}$, and $DT_{80\%,CaT}$ declined by 10%–30% between 0.75 and 2.5 Hz. The same data are also demonstrated as average peaks and force-calcium loops (Figures 4C and 4D). The correlation between force and CaT data at different frequencies demonstrates the dissociation between increasing CaT and force values above 2.0 Hz (Figure 4E). To understand the contribution of cytoplasmic expression of GCaMP6f, the experiment was repeated with non-transduced EHTs (Figure S5). This showed a maximal increase in force by +45% at 2.0 Hz. The difference in effect size is compatible with improvement of diastolic function by calcium buffering as shown for parvalbumin (Wang et al., 2013).

Omecamtiv Mecarbil

Omecamtiv mecarbil (OM) binds the catalytic domain of myosin and thereby acts as a myosin activator. OM was demonstrated to increase force and TTP while CaT remained unchanged in rat cardiomyocytes (Malik et al., 2011). Two previous studies demonstrated that the inotropic effect of OM showed reverse frequency dependency in canine myocytes (Butler et al., 2015; Horváth et al., 2017). In analogy to the demonstration of a positive FFR (Figure 4), the effect of OM (1 μM) was analyzed in the presence of ivabradine (300 nM) at frequencies between 0.75 and 2.5 Hz (Figure 5). Human iPSC-CM EHTs followed the pacing signals at all frequencies (Figures 5A and 5B). The positive inotropic effect of OM was +99% at 0.75 Hz, decreased to +54% at 1.25 Hz, and was not significant at higher frequencies. OM prolonged $TTP_{-80\%,force}$ and $RT_{80\%,force}$, with maximal effects at 1.25 (79%) and 0.75 Hz (35%), respectively, with progressively smaller effects at higher stimulation rates (Figures 5A and 5C). CaT amplitude remained unchanged, while $TTP_{-80\%,CaT}$ and $DT_{80\%,CaT}$ were maximally increased by ∼30% and 24% at 1.25 and 1.0 Hz, respectively, with smaller or no effects at higher stimulation rates (Figures 5B and 5C).

DISCUSSION

This study describes an advanced test system to analyze CaT and force in hiPSC-CM EHTs. The main findings are (1) demonstration of a temporal sequence of CaT amplitude preceding force amplitude; (2) insignificant contribution of motion artifact, demonstrated by lack of CaT change in the presence of contraction-abrogating afterload enhancement; (3) specific effects of indicator compounds on force and CaT, precisely replicating known mechanisms of action; (4) positive force-frequency and CaT-frequency relationships in the range of the physiological human heart beat; and (5) verification of a reverse correlation between frequency and inotropic effect of OM.

In a previous study, we demonstrated CaT analysis in hiPSC EHTs based on FURA-2 loading (Stoehr et al., 2014). However, variability in loading and sensitivity to washout during concentration-response curve analysis introduced artifacts that substantially compromised the use of this approach. The use of GECIs transduced with viral vehicles as applied in this study led to lower variability in fluorescence signals and lower sensitivity to washout. The family of GCaMP sensors is well established among GECIs (Kaestner et al., 2014). Both vectors, AAV6 and lentiviral, are sufficient to transfect hiPSC-CMs in 2D and in 3D culture. For 3D, transfection of hiPSC-CM EHTs only a few days before analysis did not lead to CaT with sufficient signal-to-noise ratio; therefore, viral transduction was performed during casting. This led to long-term, stable GCaMP6f expression for weeks. This approach entails expression of sensors during the process of EHT development with potential off-target effects and lower force developments via calcium buffering. Nevertheless, this did not

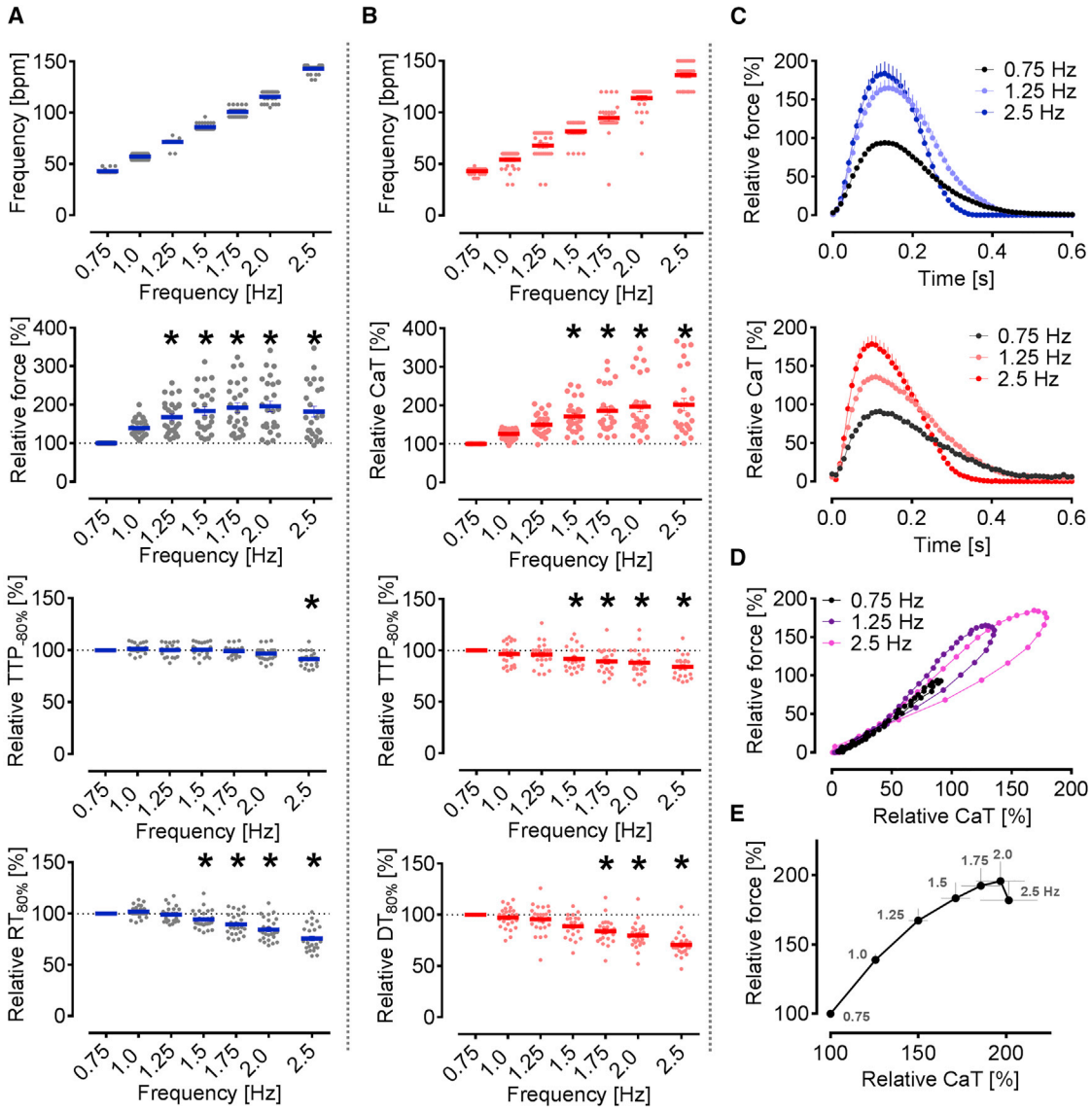

Figure 4. Force-CaT-Frequency Relationship of hiPSC EHTs Expressing GCaMP6f in the Presence of Ivabradine (300 nM)

(A) Frequency, force, time-to-peak force ($TTP_{-80\%}$), relaxation time ($RT_{80\%}$).

(B) Frequency, CaT, time-to-peak CaT ($TTP_{-80\%}$), and decay time CaT ($DT_{80\%}$).

(C and D) Depictions of selected data from (A) and (B) as (C) average force and CaT peaks and (D) force-calcium loops.

(E) Correlation of relative force and CaT amplitude values at different pacing frequencies, data from (A) and (B), means ± SEM. Depicted are plots with relative values (means ± SEM) normalized to own baseline (0.75 Hz) except frequency, depicted by absolute values; mean values are indicated by blue (force parameters) or red lines (CaT parameters). Measurements were done in modified Tyrode's solution at sub-maximal Ca^{2+} (hiPSC cell line 2 at 0.6 mM and hiPSC cell line 3 at 1.0 mM Ca^{2+}). Replicates are indicated as number of independent samples; number of hiPSC cell lines; number of repeated measurements (N; nl; nm); N was used for statistics, n = 26; 2; 3.

Statistical analysis was performed on data normalized to average baseline (0.75 Hz), one way ANOVA with Dunnett's posttest versus 0.75 Hz, *p < 0.05. See also Figure S5.

seem to be relevant, since development of force in GCaMP EHTs was not different from that in GCaMP-free EHTs. Also, non-linearity of signal intensity and non-ratiometric measurement are potential disadvantages of this approach (Rose et al., 2014). Slow kinetics of genetically encoded versus dye-based indicators are described, and GCaMP6f was developed to overcome this limitation of earlier GCaMP generations (Chen et al., 2013). Despite this improvement, time-to-CaT amplitude is reached slower than with dyes. In consequence, force-calcium loops

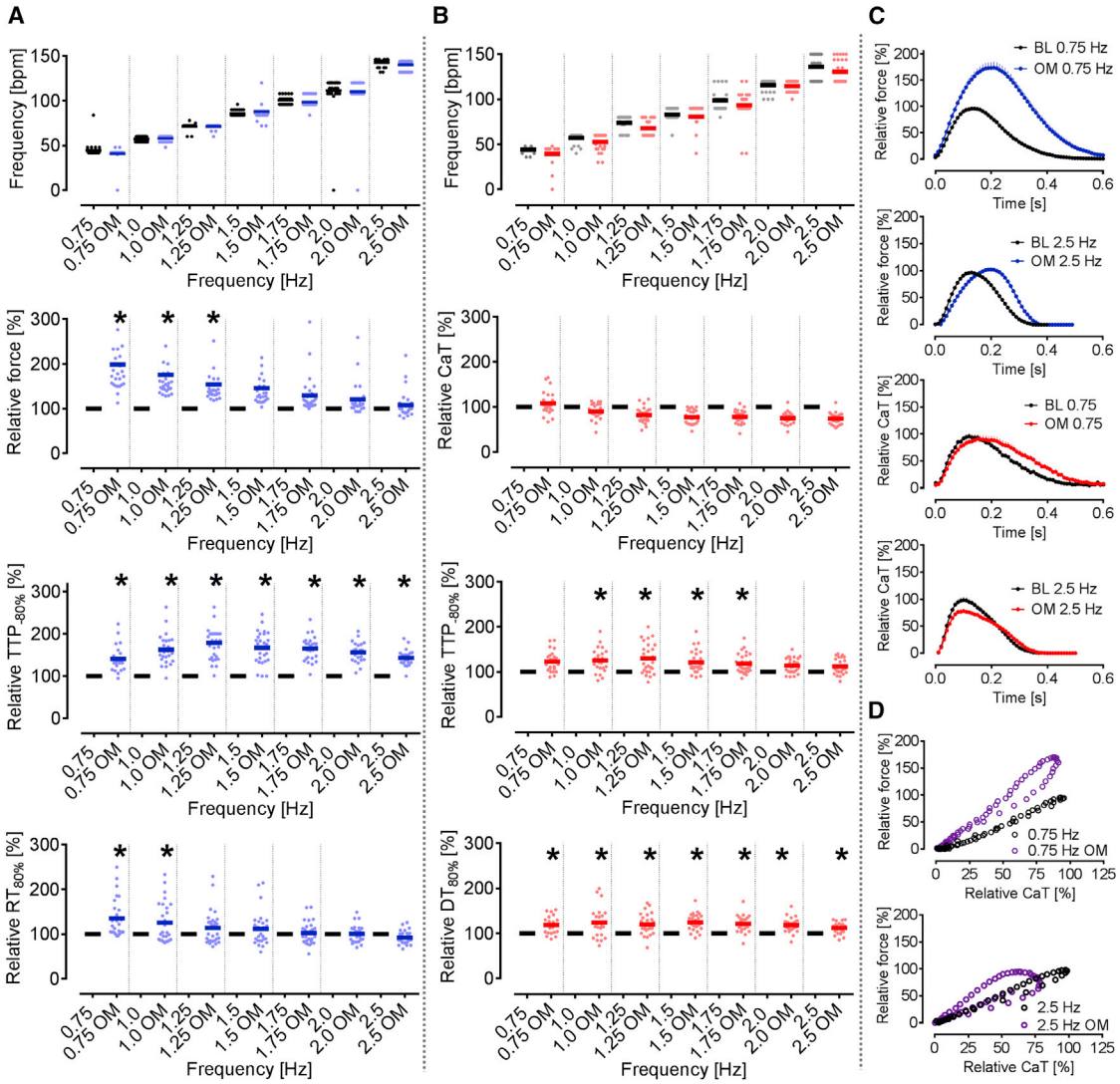

Figure 5. Effect of Omecamtiv Mecarbil (1 μM) on Contraction Force and CaT at Different Stimulation Frequencies in the Presence of Ivabradine (300 nM)

(A) Frequency, force, time-to-peak force ($TTP_{-80\%}$), relaxation time ($RT_{80\%}$).

(B) Frequency, CaT, time-to-peak CaT ($TTP_{-80\%}$), and calcium decay time ($DT_{80\%}$).

(C) Depictions of selected data from (A) and (B) as average force and CaT peaks.

(D) Depictions of selected data from (A) and (B) as force-calcium loops. Depicted are scatterplots with relative values (means ± SEM) normalized to own baseline (respective pacing frequency in the presence of ivabradine and absence of OM), except frequency, depicted by absolute values. Graphs represent values at baseline (black lines and dots) and after OM incubation (force parameters, blue lines and dots; CaT parameters, red lines and dots); lines represent mean values. Measurements were done in modified Tyrode's solution at submaximal Ca^{2+} (hiPSC cell line 2 at 0.6 mM and hiPSC cell line 3 at 1.0 mM Ca^{2+}), n = 27; 2; 3; replicates are indicated as number of independent samples; number of hiPSC cell lines; number of repeated measurements (N; nl; nm); N was used for statistics.

Two-way ANOVA with Sidak's multiple comparisons posttest versus baseline at respective frequency, *p < 0.05.

from dye-based recordings show an initial phase of calcium rise and a second phase of force increase after calcium amplitude is reached (Stoehr et al., 2014), while these phases are merged in loops from GCaMP6f recordings.

Motion artifacts in CaT analysis of contracting muscles result from increase in fluorescence signal detection due to tissue compaction during contraction, but not higher cytoplasmic calcium concentration (Cleemann and Morad, 1991). Hence, the kinetics of motion artifacts closely follow the kinetics of contraction. The difference in CaT and force kinetics, the dominant change in force in the presence of afterload enhancement and the myofilament calcium

sensitizer EMD-57033, suggests that integrating the CaT signal from a defined area in the center of the EHT does not lead to relevant motion artifacts.

Characterization of indicator compounds revealed distinct, compound-specific effects on force and CaT. Notably, CaT amplitudes (isoprenaline, digoxin) and kinetics (isoprenaline, digoxin, Bay K-8644) were altered for compounds with inotropic effects. The lack of Bay K-8644-mediated increase in CaT amplitude at 300 nM is in concordance with past studies on this compound in hamster cardiomyocyte preparations and hiPSC-CMs (Cerignoli et al., 2012; Sen et al., 1990). Likewise, the positive inotropic effect of the myofilament calcium sensitizer EMD-57033 was not associated with any changes in CaT, similar to past reports in rat papillary muscles (Ishitani et al., 2001). Digoxin-mediated inhibition of sodium/potassium ATPase increased calcium load and led to a biphasic response. The increase in CaT and force amplitude at 300 nM was followed by a toxic effect at 1.0 μM in analogy with past reports on human ventricular myocardium (Näbauer and Erdmann, 1987) and chick embryonic myocardial myocytes (Toseland et al., 1996).

The lack of a positive FFR in hiPSC-CM EHTs in past reports (Mannhardt et al., 2016) was interpreted as an indicator of cardiomyocyte immaturity. Notably, a positive FFR in the human non-failing heart in past reports was demonstrated between 0.2 and 2.9 Hz (Mulieri et al., 1992), 0.5–2.5 Hz (Pieske et al., 1999), and 0.1–2.5 Hz (Schmidt et al., 1995). This is in line with the recognition that a positive FFR prevails in the range of the physiological heart rate for the respective species (Endoh, 2004). In agreement with this, rabbit and rat trabeculae showed a positive FFR at 1 to 4 Hz and 4 to 8 Hz, respectively (Monasky and Janssen, 2009). Ivabradine has been used at a concentration (300 nM) that is not known to inhibit other ion currents. The half-maximal inhibitory concentration (IC_{50}) value of ivabradine needed to inhibit I_f current in CHO cells was 0.54 μM (Thollon et al., 2007). Compatible with this finding, it reduced spontaneous beating in hiPSC EHTs by 50% at 300 nM (Mannhardt et al., 2016). At higher concentrations (e.g., 10 μM) ivabradine is not selective anymore and reduces I_K and $I_{Ca,L}$ (Bois et al., 1996). Reduction of baseline frequency with ivabradine in hiPSC-CM EHTs unmasked a positive FFR in a beating range close to the physiological human heartbeat, indicating that the complex calcium-handling machinery required for this physiological response is established in this model. Furthermore, a positive correlation between CaT and frequency and a dissociation of the force-frequency and CaT-frequency relationship at high pacing frequencies was demonstrated, which is in line with past reports on FFRs in different mammalian species (Gwathmey et al., 1990; Monasky and Janssen, 2009). The smaller FFR effect size versus adult myocardium (Monasky and Janssen, 2009) is compatible with an intermediate state of maturation. This is also in line with lower baseline force values for EHT versus adult myocardium. Nevertheless, relative changes to physiological stimuli and pharmacological interventions replicated findings in adult heart tissue (Mannhardt et al., 2016). In addition, the dissociation of increasing CaT amplitude values from plateauing force amplitude values at the upper end of the physiological beating range is another characteristic of FFRs in mammalian species (Endoh, 2004; Gwathmey and Hajjar, 1990) and could be replicated in this model. These data strengthen the finding that many physiological aspects of human heart tissue are replicated in the hiPSC-CM EHT model (Mannhardt et al., 2016), but also point to the fact that sophisticated experimental conditions are required in some cases to demonstrate them.

The principle of lowering baseline frequency in hiPSC-CM EHTs with ivabradine to demonstrate FFR was taken forward to analyze the effect of OM. The data confirm the reverse frequency dependency of the inotropic effect previously reported in two canine models (Butler et al., 2015; Horváth et al., 2017). Furthermore, the lack of increase in CaT amplitude is in agreement with myosin activation as a primary mode of action. The nature of the increase in $TTP_{-80\%,CaT}$ and $DT_{80\%,CaT}$ is not known; similar trends were, however, recently reported in a canine myocyte model (Horváth et al., 2017). Taken together, several physiological and pharmacological positive inotropic mechanisms were presented in this study, which modify either calcium handling (Bay K-8644, digoxin, FFR) or myofilaments (EMD-57033, OM) and are therefore associated with a variety of CaT amplitude and kinetics alterations, demonstrating the added value of a combined analysis.

Limitations of this study are (1) the sequential and not parallel recording of CaT and force, which increases experimental complexity and allows for measurements only at steady state and not of short and transient effects; (2) the slower on-kinetics of GCaMP6f (versus calcium-sensitive dyes), reducing the significance of $TTP_{-80\%,CaT}$; and (3) the experimental approach to transduce EHTs during casting, which reduces experimental flexibility.

In summary, this study describes a test system to monitor CaT and force in hiPSC-CM EHTs to study the physiology and pharmacology of cardiomyocytes with high accuracy.

EXPERIMENTAL PROCEDURES

Expansion and Differentiation of Human Induced Pluripotent Stem Cells

Cardiac differentiation of hiPSCs was performed as recently described (Breckwoldt et al., 2017). In brief, hiPSCs were expanded on Geltrex-coated cell culture vessels with FTDA medium, and splitting was performed with EDTA. Formation of embryoid bodies

was performed in spinner flasks, and differentiation was conducted in Pluronic F-127-coated cell culture vessels with a sequential administration of growth factor- and small-molecule-based cocktails to induce mesodermal progenitors, cardiac progenitors, and cardiomyocytes. Dissociation of differentiated cardiomyocytes was performed with collagenase, and dissociated cardiomyocytes were analyzed for cardiac differentiation efficiency by flow cytometry (cardiac troponin T) and subjected to EHT generation. All procedures involving the generation and analysis of hiPSC lines were approved by the local ethics committee in Hamburg (Az PV4798, 28.10.2014).

Sensor Plasmid, AAV and Lentiviral Vector Production, and Transduction of Cardiomyocytes

The details are described in the Supplemental Experimental Procedures.

Generation of Human Engineered Heart Tissue and GCaMP6f Transduction

Human EHTs were generated as recently described (Breckwoldt et al., 2017). Frozen or freshly dissociated hiPSC-CMs were counted and a master mix was prepared. Nunc 24-well plates were used to generate casting molds with liquid agarose (2% in PBS, 1.5 mL per well) and Teflon spacers (EHT Technologies). After agarose solidification (10 min), Teflon spacers were removed, and PDMS racks (EHT Technologies) were placed on 24-well plates so that pairs of PDMS posts reached into each agarose casting mold. The master mix (97 μL) was briefly mixed with thrombin (3 μL) and pipetted into one agarose casting mold. This pipetting step was repeated for each casting mold with a new pipette tip to avoid thrombin carryover and fibrin polymerization in the pipette tip. Full plates of EHTs were incubated for 90 min in the incubator and 200–300 μL of EHT medium was added per well to ease removal of EHTs from agarose casting molds. PDMS racks with EHTs were transferred from the casting plate to an additional 24-well plate, filled with EHT medium (1.5 mL/well), 2 h after casting. EHT medium was changed on Mondays, Wednesdays, and Fridays. Contractions of single cardiomyocytes were usually visible after 3–5 days, larger networks of cardiomyocytes started beating after 7–10 days, and synchronous contraction of the entire EHT was observed after 14 days. Transduction of human EHTs with GCaMP6f was performed by adding AAV6 particles (originally, MOI of 7×10^4 and 7×10^5 [genomic titer] were tested (Figure 1E), and for follow-up experiments, an MOI of 1×10^6 [genomic titer, Figure 1F] was chosen) or lentiviral particles (MOI of 0.3, functional titer) into the master mix during casting. Analysis of CaT and force was performed on day 20–70.

Recording of Contractility and Calcium Transients

Automated sequential video-optical analyses for force and fluorescence-based CaT recordings under frequency control by electrical pacing (as recently described by Hirt et al., 2014) were performed as recently described (Stoehr et al., 2014). An automated xy stage was built on an inverted fluorescence microscopy stage (Axiovert, Zeiss). The automated xy stage was covered with a light-tight temperature- and CO_2-controlled homemade incubation chamber. A camera for force recording was connected to the front port of the microscope. A mercury lamp and GFP filter set were installed for fluorescent light excitation. The side port of the microscope was connected via beam splitter to a long-pass filter/photomultiplier and a camera to control the position for fluorescence recording. For the analysis, human EHTs were transferred into a cell-imaging 24-well plate (Eppendorf) equipped with graphite-based pacing electrodes. The plate was placed into the 24-well inlet of the microscope, and the plastic box covering the microscope was closed. The objective focus of the microscope served as the z axis on this stage. A customized software was used to control microscope settings, xyz coordinates, and objective revolver position. The xyz coordinates were defined and saved in the software for each EHT to perform automated force (1.25× objective) and CaT (10× objective) recordings.

Force was analyzed by video-optical recording as described in the past (Hansen et al., 2010; Mannhardt et al., 2016; Schaaf et al., 2011). Software-based automated video-optical recording of EHT contractility was started. A video file was generated for each EHT (100 frames per second). A customized software algorithm automatically identified top and bottom ends of the EHT contour and followed these positions during the course of the contraction. Force was then calculated based on EHT shortening and the elastic propensity and geometry of the PDMS posts to which the EHTs were attached. Raw traces were plotted with force (y axis) over time (x axis), filtered (Gaussian filter), and baseline corrected. Contraction peak amplitudes were identified based on predefined contraction peak criteria and marked with a green square for visual quality control. Average values for force, frequency, and parameters of kinetics were calculated and summarized in a report file. This report also contained force graphs in which the electrical pacing signal was indicated with a vertical blue line (Figure S2A).

GCaMP fluorescence intensity was measured as a surrogate for CaT. The emitted fluorescent light from the GCaMP-transduced EHT in the well was reflected by the dichroic mirror and band-pass-filtered and sensed by the photomultiplier tube (PMT). The PMT converted light intensities into electrical signals and forwarded the signals (frame rate: 100 frames per second) to the customized software. Raw traces were plotted with intensities (y axis) over time (x axis), filtered (Gaussian filter), and baseline corrected. In filtered traces an automated peak identification algorithm identified CaT peaks and marked them with a green square for visual quality control. From there, CaT amplitude and kinetics were automatically calculated and summarized as mean values ± SD in a report file. This report also contained CaT graphs in which the electrical pacing signal was indicated with a vertical blue line (Figure S2A). CaT recordings were performed between 3 and 10 s. CaT that were incompletely displayed on this graph were excluded from the analysis. Signal-to-noise ratio was calculated based on CaT amplitudes and background signal intensity in original recordings (Figure S2A). Representativity of the area for CaT signal integration was presumed based on the homogeneity of the EHT structure and the calculation of mean values from 10 to 26 individual EHTs for the experiments presented in this paper.

Positive inotropic compounds were analyzed in Tyrode's solution at submaximal extracellular calcium concentrations close to the EC_{50} values for the respective EHT batch, which were in the range of 0.5–1.0 mM calcium. For this, first, baseline force

at 1.8 mM calcium was analyzed, and extracellular calcium was washed out until half-maximal force values were recorded. Afterward, recordings were done at baseline and 20–30 min after compound incubation. For the analysis, only contraction or CaT recordings were considered, in which the contractions/CaT followed the pacing frequency. Recordings in which the EHTs were beating at a higher frequency than the pacing signal were excluded from the analysis. In case of artifacts or baseline drift during CaT recording, offline analysis was performed to exclude part of the recordings. Since CaT peaks were sometimes cut by this procedure and incomplete peaks were excluded from the analysis, recalculated frequency values after offline analysis showed lower values than actual pacing frequency.

Histological Analysis

Details are described in the Supplemental Experimental Procedures.

Statistical Analysis

Statistical differences were determined by paired t test, one-way ANOVA with Dunnett's/Tukey's/Bonferroni's multiple comparisons posttest, and two-way ANOVA with Sidak's multiple comparisons posttest versus baseline as indicated in figure legends. Data presented within the text are listed as means ± SEM.

ACCESSION NUMBERS

BioSD: SAMEA6235102, SAMEA6248848.

SUPPLEMENTAL INFORMATION

Supplemental Information can be found online at https://doi.org/10.1016/j.stemcr.2019.12.011.

AUTHOR CONTRIBUTIONS

T.E. and A.H. conceived and organized the project and wrote the manuscript; U.S. designed and performed the experiments and analyzed data, with contributions from I.B. and I.M. All authors discussed the results and commented on the manuscript.

ACKNOWLEDGMENTS

We thank Thomas Schulze, Birgit Klampe, Bärbel Ulmer, Anika Knaust, Tessa Werner, Mirja Schulze, Kaja Yorgan, Pierre Bobin, Giulia Mearini, Marina Reinsch, Maksimilian Prondzynski, Aya Shibamiya, and Christiane Neuber, for their support with stem cell culture and cardiomyocyte differentiation, and Kristin Hartmann, UKE Histology Core Facility, for her support with immunohistochemistry. This study was supported by the British National Centre for the Replacement Refinement & Reduction of Animals in Research (NC3Rs CRACK IT grant 35911-259146), the European Research Council, European Union (ERC-AG IndivuHeart), the Deutsche Forschungsgemeinschaft, Germany (DFG Es 88/12-1, DFG HA 3423/5-1), the German Ministry of Education and Research (BMBF), the German Centre for Cardiovascular Research (DZHK), and Freie und Hansestadt Hamburg, Germany. T.E., A.H., and I.M. are co-founders of EHT Technologies.

Received: March 25, 2019
Revised: December 17, 2019
Accepted: December 18, 2019
Published: January 16, 2020

REFERENCES

Bers, D.M., Morotti, S., Greenstein, J.L., Anderson, M.E., and Grueter, C. (2014). Ca 2+ current facilitation is CaMKII-dependent and has arrhythmogenic consequences. Front. Pharmacol. *5*, 144.

Bielawski, K.S., Leonard, A., Bhandari, S., Murry, C.E., and Sniadecki, N.J. (2016). Real-time force and frequency analysis of engineered human heart tissue derived from induced pluripotent stem cells using magnetic sensing. Tissue Eng. Part C Methods *22*, 932–940.

Biermann, M., Rubart, M., Moreno, A., Wu, J., Josiah-Durant, A., and Zipes, D.P. (1998). Differential effects of cytochalasin D and 2,3 butanedione monoxime on isometric twitch force and transmembrane action potential in isolated ventricular muscle: implications for optical measurements of cardiac repolarization. J. Cardiovasc. Electrophysiol. *9*, 1348–1357.

Bois, P., Bescond, J., Renaudon, B., and Lenfant, J. (1996). Mode of Action of Bradycardic Agent, S 16257, on Ionic Currents of Rabbit Sinoatrial Node Cells (Stockton Press).

Breckwoldt, K., Letuffe-Brenière, D., Mannhardt, I., Schulze, T., Ulmer, B., Werner, T., Benzin, A., Klampe, B., Reinsch, M.C., Laufer, S., et al. (2017). Differentiation of cardiomyocytes and generation of human engineered heart tissue. Nat. Protoc. *12*, 1177–1197.

Brixius, K., Reicke, S., Reuter, H., and Schwinger, R.H.G. (2002). Effects of the Ca2+ sensitizers EMD 57033 and CGP 48506 on myocardial contractility and Ca2+ transients in human ventricular and atrial myocardium. Z. Kardiol. *91*, 312–318.

Brixius, K., Wollmer, A., Bölck, B., Mehlhorn, U., and Schwinger, R.H.G. (2003). Ser16-, but not Thr17-phosphorylation of phospholamban influences frequency-dependent force generation in human myocardium. Pflugers Arch. *447*, 150–157.

Butler, L., Cros, C., Oldman, K.L., Harmer, A.R., Pointon, A., Pollard, C.E., and Abi-Gerges, N. (2015). Enhanced characterization of contractility in cardiomyocytes during early drug safety assessment. Toxicol. Sci. *145*, 396–406.

Cashman, T.J., Josowitz, R., Johnson, B.V., Gelb, B.D., and Costa, K.D. (2016). Human engineered cardiac tissues created using induced pluripotent stem cells reveal functional characteristics of BRAF-mediated hypertrophic cardiomyopathy. PLoS One *11*, e0146697.

Cerignoli, F., Charlot, D., Whittaker, R., Ingermanson, R., Gehalot, P., Savchenko, A., Gallacher, D.J., Towart, R., Price, J.H., McDonough, P.M., et al. (2012). High throughput measurement of Ca^{2+} dynamics for drug risk assessment in human stem cell-derived cardiomyocytes by kinetic image cytometry. J. Pharmacol. Toxicol. Methods *66*, 246–256.

Chen, T.W., Wardill, T.J., Sun, Y., Pulver, S.R., Renninger, S.L., Baohan, A., Schreiter, E.R., Kerr, R.A., Orger, M.B., Jayaraman, V., et al. (2013). Ultrasensitive fluorescent proteins for imaging neuronal activity. Nature *499*, 295–300.

Cleemann, L., and Morad, M. (1991). Role of Ca2+ channel in cardiac excitation-contraction coupling in the rat: evidence from Ca2+ transients and contraction. J. Physiol. *432*, 283–312.

Endoh, M. (2004). Force–frequency relationship in intact mammalian ventricular myocardium: physiological and pathophysiological relevance. Eur. J. Pharmacol. *500*, 73–86.

Gwathmey, J.K., and Hajjar, R.J. (1990). Intracellular calcium related to force development in twitch contraction of mammalian myocardium. Cell Calcium *11*, 531–538.

Gwathmey, J.K., Slawsky, M.T., Hajjar, R.J., Briggs, G.M., and Morgan, J.P. (1990). Role of intracellular calcium handling in force-interval relationships of human ventricular myocardium. J. Clin. Invest. *85*, 1599–1613.

Haizlip, K.M., Milani-Nejad, N., Brunello, L., Varian, K.D., Slabaugh, J.L., Walton, S.D., Gyorke, S., Davis, J.P., Biesiadecki, B.J., and Janssen, P.M.L. (2015). Dissociation of calcium transients and force development following a change in stimulation frequency in isolated rabbit myocardium. Biomed. Res. Int. *2015*, 468548.

Hansen, A., Eder, A., Bönstrup, M., Flato, M., Mewe, M., Schaaf, S., Aksehirlioglu, B., Schwörer, A., Uebeler, J., and Eschenhagen, T. (2010). Development of a drug screening platform based on engineered heart tissue. Circ. Res. *107*, 35–44.

Hinson, J.T., Chopra, A., Lowe, A., Sheng, C.C., Gupta, R.M., Kuppusamy, R., O'Sullivan, J., Rowe, G., Wakimoto, H., Gorham, J., et al. (2016). Integrative analysis of PRKAG2 cardiomyopathy iPS and microtissue models identifies AMPK as a regulator of metabolism, survival, and fibrosis. Cell Rep. *17*, 3292–3304.

Hirt, M.N., Sörensen, N.A., Bartholdt, L.M., Boeddinghaus, J., Schaaf, S., Eder, A., Vollert, I., Stöhr, A., Schulze, T., Witten, A., et al. (2012). Increased afterload induces pathological cardiac hypertrophy: a new in vitro model. Basic Res. Cardiol. *107*, 1–16.

Hirt, M.N., Boeddinghaus, J., Mitchell, A., Schaaf, S., Börnchen, C., Müller, C., Schulz, H., Hubner, N., Stenzig, J., Stoehr, A., et al. (2014). Functional improvement and maturation of rat and human engineered heart tissue by chronic electrical stimulation. J. Mol. Cell. Cardiol. *74*, 151–161.

Horváth, B., Szentandrássy, N., Veress, R., Almássy, J., Magyar, J., Bányász, T., Tóth, A., Papp, Z., and Nánási, P.P. (2017). Frequency-dependent effects of omecamtiv mecarbil on cell shortening of isolated canine ventricular cardiomyocytes. Naunyn. Schmiedebergs. Arch. Pharmacol. *390*, 1239–1246.

Ishitani, T., Hattori, Y., Sakuraya, F., Onozuka, H., Makino, T., Matsuda, N., Gando, S., and Kemmotsu, O. (2001). Effects of Ca2+ sensitizers on contraction, [Ca2+]i transient and myofilament Ca2+ sensitivity in diabetic rat myocardium: potential usefulness as inotropic agents. J. Pharmacol. Exp. Ther. *298*, 613–622.

Jackman, C.P., Carlson, A.L., and Bursac, N. (2016). Dynamic culture yields engineered myocardium with near-adult functional output. Biomaterials *111*, 66–79.

Kaestner, L., Scholz, A., Tian, Q., Ruppenthal, S., Tabellion, W., Wiesen, K., Katus, H.A., Müller, O.J., Kotlikoff, M.I., and Lipp, P. (2014). Genetically encoded Ca2+ indicators in cardiac myocytes. Circ. Res. *114*, 1623–1639.

Kensah, G., Roa Lara, A., Dahlmann, J., Zweigerdt, R., Schwanke, K., Hegermann, J., Skvorc, D., Gawol, A., Azizian, A., Wagner, S., et al. (2013). Murine and human pluripotent stem cell-derived cardiac bodies form contractile myocardial tissue in vitro. Eur. Heart J. *34*, 1134–1146.

Képiró, M., Várkuti, B.H., Végner, L., Vörös, G., Hegyi, G., Varga, M., and Málnási-Csizmadia, A. (2014). Para-nitroblebbistatin, the non-cytotoxic and photostable myosin II inhibitor. Angew. Chem. Int. Ed. *53*, 8211–8215.

Klabunde, R.E. (2012). Cardiovascular Physiology Concepts (Lippincott Williams & Wilkins).

Krishna, A., Valderrábano, M., Palade, P.T., and Clark, J.W. (2013). Rate-dependent Ca 2+ signalling underlying the force-frequency response in rat ventricular myocytes: a coupled electromechanical modeling study. Theor. Biol. Med. Model. *10*, 54.

Leonard, A., Bertero, A., Powers, J.D., Beussman, K.M., Bhandari, S., Regnier, M., Murry, C.E., and Sniadecki, N.J. (2018). Afterload promotes maturation of human induced pluripotent stem cell derived cardiomyocytes in engineered heart tissues. J. Mol. Cell. Cardiol. *118*, 147–158.

Li, P., Geng, X., Jiang, H., Caccavano, A., Vicini, S., and Wu, J.Y. (2019). Measuring sharp waves and oscillatory population activity with the genetically encoded calcium indicator GCaMP6f. Front. Cell. Neurosci. *13*, 1–15.

Malik, F.I., Hartman, J.J., Elias, K.A., Morgan, B.P., Rodriguez, H., Brejc, K., Anderson, R.L., Sueoka, S.H., Lee, K.H., Finer, J.T., et al. (2011). Cardiac myosin activation: a potential therapeutic approach for systolic heart failure. Science *331*, 1439–1443.

Mannhardt, I., Breckwoldt, K., Letuffe-brenière, D., Schaaf, S., Neuber, C., Benzin, A., Werner, T., Eder, A., Klampe, B., Christ, T., et al. (2016). Human engineered heart tissue: analysis of contractile force. Stem Cell Rep. *7*, 29–42.

Mills, R.J., Titmarsh, D.M., Koenig, X., Parker, B.L., Ryall, J.G., Quaife-Ryan, G.A., Voges, H.K., Hodson, M.P., Ferguson, C., Drowley, L., et al. (2017). Functional screening in human cardiac organoids reveals a metabolic mechanism for cardiomyocyte cell cycle arrest. Proc. Natl. Acad. Sci. U S A *114*, E8372–E8381.

Monasky, M.M., and Janssen, P.M.L. (2009). The positive force-frequency relationship is maintained in absence of sarcoplasmic reticulum function in rabbit, but not in rat myocardium. J. Comp. Physiol. B Biochem. Syst. Environ. Physiol. *179*, 469–479.

Mulieri, L.A., Hasenfuss, G., Leavitt, B., Allen, P.D., and Alpert, N.R. (1992). Altered myocardial force-frequency relation in human heart failure. Circulation *85*, 1743–1750.

Näbauer, M., and Erdmann, E. (1987). Reversal of toxic and non-toxic effects of digoxin by digoxin-specific Fab fragments in isolated human ventricular myocardium. Klin. Wochenschr. *65*, 558–561.

Nunes, S.S., Miklas, J.W., Liu, J., Aschar-Sobbi, R., Xiao, Y., Zhang, B., Jiang, J., Massé, S., Gagliardi, M., Hsieh, A., et al. (2013). Biowire: a platform for maturation of human pluripotent stem cell-derived cardiomyocytes. Nat. Methods *10*, 781–787.

Perreault, C.L., Shannon, R.P., Komamura, K., Vatner, S.F., and Morgan, J.P. (1992). Abnormalities in intracellular calcium

regulation and contractile function in myocardium from dogs with pacing-induced heart failure. J. Clin. Invest. *89*, 932–938.

Pieske, B., Maier, L.S., Bers, D.M., and Hasenfuss, G. (1999). Ca2+ handling and sarcoplasmic reticulum Ca2+ content in isolated failing and nonfailing human myocardium. Circ. Res. *85*, 38–46.

Rao, L., Qian, Y., Khodabukus, A., Ribar, T., and Bursac, N. (2018). Engineering human pluripotent stem cells into a functional skeletal muscle tissue. Nat. Commun. *9*, 126.

Ronaldson-Bouchard, K., Ma, S.P., Yeager, K., Chen, T., Song, L., Sirabella, D., Morikawa, K., Teles, D., Yazawa, M., and Vunjak-Novakovic, G. (2018). Advanced maturation of human cardiac tissue grown from pluripotent stem cells. Nature *556*, 239–243.

Rose, T., Goltstein, P.M., Portugues, R., and Griesbeck, O. (2014). Putting a finishing touch on GECIs. Front. Mol. Neurosci. *7*, 88.

Ruan, J.-L., Tulloch, N.L., Razumova, M.V., Saiget, M., Muskheli, V., Pabon, L., Reinecke, H., Regnier, M., and Murry, C.E. (2016). Mechanical stress conditioning and electrical stimulation promote contractility and force maturation of induced pluripotent stem cell-derived human cardiac tissue. Circulation *134*, 1557–1567.

Schaaf, S., Shibamiya, A., Mewe, M., Eder, A., Stöhr, A., Hirt, M.N., Rau, T., Zimmermann, W.-H., Conradi, L., Eschenhagen, T., et al. (2011). Human engineered heart tissue as a versatile tool in basic research and preclinical toxicology. PLoS One *6*, e26397.

Schmidt, U., Hajjar, R.J., and Gwathmey, J.K. (1995). The force-interval relationship in human myocardium. J. Card. Fail. *1*, 311–321.

Sen, L.Y., O'Neill, M., Marsh, J.D., and Smith, T.W. (1990). Inotropic and calcium kinetic effects of calcium channel agonist and antagonist in isolated cardiac myocytes from cardiomyopathic hamsters. Circ. Res. *67*, 599–608.

Stoehr, A., Neuber, C., Baldauf, C., Vollert, I., Friedrich, F.W., Flenner, F., Carrier, L., Eder, A., Schaaf, S., Hirt, M.N., et al. (2014). Automated analysis of contractile force and Ca2+ transients in engineered heart tissue. Am. J. Physiol. Heart Circ. Physiol. *306*, H1353–H1363.

Thollon, C., Bedut, S., Villeneuve, N., Cogé, F., Piffard, L., Guillaumin, J.P., Brunel-Jacquemin, C., Chomarat, P., Boutin, J.A., Peglion, J.L., et al. (2007). Use-dependent inhibition of hHCN4 by ivabradine and relationship with reduction in pacemaker activity. Br. J. Pharmacol. *150*, 37–46.

Tiburcy, M., Hudson, J.E., Balfanz, P., Schlick, S., Meyer, T., Chang Liao, M.-L., Levent, E., Raad, F., Zeidler, S., Wingender, E., et al. (2017). Defined engineered human myocardium with advanced maturation for applications in heart failure modeling and repair. Circulation *135*, 1832–1847.

Toseland, C.D., Seaman, C.W., Francis, I., White, D.J., and Earl, L.K. (1996). Study of the effects of cardiovascular drugs in heart cell cultures. Toxicol. In Vitro *10*, 765–773.

Tulloch, N.L., Muskheli, V., Razumova, M.V., Korte, F.S., Regnier, M., Hauch, K.D., Pabon, L., Reinecke, H., and Murry, C.E. (2011). Growth of engineered human myocardium with mechanical loading and vascular coculture. Circ. Res. *109*, 47–59.

Wang, W., Barnabei, M.S., Asp, M.L., Heinis, F.I., Arden, E., Davis, J., Braunlin, E., Li, Q., Davis, J.P., Potter, J.D., et al. (2013). Noncanonical EF-hand motif strategically delays Ca2+ buffering to enhance cardiac performance. Nat. Med. *19*, 305–312.

Zhao, Y., Rafatian, N., Feric, N.T., Cox, B.J., Aschar-Sobbi, R., Wang, E.Y., Aggarwal, P., Zhang, B., Conant, G., Ronaldson-Bouchard, K., et al. (2019). A platform for generation of chamber-specific cardiac tissues and disease modeling. Cell *176*, 913–927.e18.